Title
Anti-inflammatory Drug Eluting Patches for Treatment of Ocular Injuries

Author
Chen, Xi

Publication Date
2021

Peer reviewed|Thesis/dissertation

UNIVERSITY OF CALIFORNIA

Los Angeles

Anti-inflammatory Drug Eluting Patches for Treatment of Ocular Injuries

A thesis submitted in partial satisfaction

of the requirements for the degree Master of Science

in Chemical Engineering

by

Xi Chen

2021

ABSTRACT OF THE THESIS

Anti-inflammatory Drug Eluting Patches

for Treatment of Ocular Injuries

by

Xi Chen

Master of Science in Chemical Engineering

University of California, Los Angeles, 2021

Professor Nasim Annabi, Chair

Ocular inflammations are commonly associated with eye diseases, injuries, and postoperative complications, which affect many patients worldwide. However, effective and sustained ocular delivery of therapeutics remains a challenge because of ocular structural barriers. Herein, we engineered a photocrosslinkable adhesive patch (GelPatch) incorporating micelles loaded with anti-inflammatory drugs. GelPatch hydrogels are composed of two polymers, gelatin methacryloyl (GelMA) and hyaluronic acid-glycidyl methacrylate (HAGM). Anti-inflammatory corticosteroids are loaded in micelles composed of poly(ethylene glycol)-b-poly[N-(2-hydroxypropyl) methacrylamide-oligolactates] (mPEG-b-p(HPMAm-Lac_n)) diblock copolymers. The adequate adhesive strength of GelPatch with proper swelling and mechanical properties provides adhesion to the ocular surface and the incorporation of micelles provides a sustained release profile of drugs

in 15 days. *In vitro* assays showed that micelle loaded GelPatch had good biocompatibility and cell adherence and growth. The subcutaneous implantation of the micelle loaded GelPatch in rats further confirmed its *in vivo* biocompatibility and appropriate stability within 28 days. This non-invasive, adhesive and biocompatible drug eluting patch provides site-targeted delivery with lower dosage requirements to ensure better patient compliance. Such ocular drug delivery platform can be used for treatment of different ocular anterior segment diseases and injuries such as conjunctivitis, blepharitis, and postoperative care.

The thesis of Xi Chen is approved.

Junyoung O. Park

Panagiotis D. Christofides

Nasim Annabi, Committee Chair

University of California, Los Angeles

2021

Table of Contents

List of Figures

Acknowledgements

I would like to thank my advisor Professor Nasim Annabi for giving me the opportunity to learn and explore drug delivery and biomaterials research as a Master's student in her lab. Throughout my journey, she gave me great guidance, support and encouragement.

I would like to thank my mentor Shima Gholizadeh. This project would not be done without her teaching me the concepts and experiments in the first place. It is so much fun working with her.

Thanks to Yangcheng Liu, Mahsa Ghovvati, and Azadeh Mostafavi for helping me with this project.

Thanks to Junyoung O. Park, Samanvaya Srivastava, Dante Simonetti and many other UCLA faculty for sharing knowledge and wisdom throughout my graduate studies.

Thanks to all my lab colleagues. I can always learn things from them.

I would like to thank Professor Junyoung O. Park and Professor Panagiotis D. Christofides for being my Master's thesis committee.

Lastly, I would like to thank my parents and Rafael. None of these would have been possible without your support.

CHAPTER I. Introduction

Eye diseases worldwide have been a serious problem affecting many people around the world due to the increasing use of contact lens, air conditioners, long-hour staring at computers and aging, etc. These behaviors can cause dry eyes and irritations and can further develop infections and inflammations like conjunctivitis, glaucoma as well as age-related macular degeneration [1, 2]. Often times, severe eye diseases and injuries are treated with eye surgeries and post-surgery care are required to prevent inflammations. However, effective and efficient delivery of therapeutics into patient eyes remains a challenge because of several structural barriers. Due to blood-retinal barrier, systemic routes require a large dose in order to achieve a satisfactory drug concentration in intraocular tissues, which can lead to off-target systemic side effects [3]. On the other hand, local drug delivery such as the conventional topical administration (eye drops or ointments) have extremely low bioavailability of 5% due to corneal epithelium barrier and fast clearance by tear film and blinking [4]. As a result, repetitive drug applications are required, which may induce ocular hypertension and are also associated with poor patient compliance. Additionally, intraocular injection is used to circumvent the bioavailability issue. For example, surgeons use a small gauge needle to inject the medicine into the patient eyes after the surgery. However, this method is more invasive and complications such as post-operation pain, intraocular pressure spikes, and retinal detachment can arise [5]. Hence, a localized and noninvasive efficient ocular drug delivery method with good patient compliance is preferable and ocular drug-eluting patch is one of the desired platforms.

Various patch-based drug delivery systems, made of different polymers, have been developed throughout the years, but still have some drawbacks for ocular drug delivery applications. For

example, drug-eluting soft contact lenses (SCL) made of silicone polymers were successfully engineered [6]. SCL were loaded with drugs by soaking them in a concentrated drug solution, liposome loading and surface modification. However, drawbacks associated with these post-modifying SCL are the low drug loading and the potential of altering its optimal properties. Although these SCLs are designed to have good gas permeabilities, long hours of wearing SCL with constant eye movement could induce more irritation to the patients with inflammation in the first place. On the other hand, microneedle (MN)-based patches were shown to deliver drugs locally by penetrating the epithelial and stromal layers of the cornea and the sclera [7]. While deemed minimally invasive, high volume taken up and pressure of infusion could cause pain, resulting in poor patient compliance. For example, a recent Phase 1 study reported that a hollow MN injection into suprachoroidal space (a potential space between sclera and choroid) was more painful that intravitreal injection, presumably due to distension caused by the volume of the injected drugs [8]. Additionally, the uncontrolled retraction from the cornea and sclera could lead to complete removal of the MN and leakage of drugs onto the surface, lowering the effective quantity of drugs delivered into the tissue. Therefore, we envisioned the need to develop a drug loaded adhesive patch which can adhere to the ocular tissue and bypass the barrier to increase bioavailability for sustained release of therapeutics. Using biocompatible and biodegradable materials can further improve the patient compliance and the cost by reducing hospital visits for patch removal.

There are several types of ocular adhesive patches developed so far with high adhesion to ocular tissues, but these platforms mainly focused on sealing and repair of ocular injuries without incorporating a drug delivery system [16, 54]. For example, cyanoacrylate-based ocular adhesives

are used by ophthalmologists to seal eye wounds [9, 10]. Although cyanoacrylate-based ocular adhesives offer a fast and easy treatment of sealing ocular injuries, they are associated with several drawbacks including cytotoxicity, irregular rough surfaces, and non-biodegradable nature [11, 12]. Poly(ethylene glycol) (PEG)-based ocular glues, on the other hand, are biocompatible and have tunable mechanical properties and biodegradability [13]. For instance, ReSure, a PEG-based adhesive, is an FDA-approved ocular sealant used to seal corneal incisions after cataract surgery [14]. However, ReSure requires a mixing of two components and only allows a 14-17 sec application time window after mixing, which can be limited in some circumstances [15]. Moreover, fibrin sealant, a naturally derived polymer-based ocular adhesive, shows excellent biocompatibility and biodegradability but it requires a longer gelation time after application and has lower adhesive strength especially to wet surfaces. Other challenges including batch to batch product variations and the potential presence of viral contamination in the production of fibrin sealant still remain to be addressed [16].

Our team has recently developed a photocrosslinkable gelatin-based adhesive hydrogel (GelCORE), which showed high biocompatibility with good adhesion to stromal defected cornea. Before crosslinking, GelCORE remains in a liquid form to be applied directly on stromal defect, but it does not provide enough viscosity to retain onto the intact cornea surfaces. Hyaluronic acid (HA) is known as a viscoelastic and highly biocompatible glycosaminoglycan [17]. By modifying HA with photocrosslinkable groups and mixing it with GelCORE at a certain ratio, we propose to form a composite adhesive, GelPatch, with preferable viscosity before photocrosslinking and strong tissue adhesion and mechanical properties after photocrosslinking to be used as a matrix for ocular drug delivery. The noninvasive, adhesive and biocompatible GelPatch has great potential

to circumvent the drawbacks of contact lens, microneedle patches, and current available adhesives. By loading micelle (MC) solubilized anti-inflammatory drugs into GelPatch, we further investigate its capability of sustained drug release into the eye for the treatment of ocular diseases.

Topical corticosteroids are commonly used in the treatment of ocular anterior segment diseases and postoperative inflammation due to their anti-inflammatory effects [18]. Loteprednol etabonate (LE), prednisolone acetate (PA), and dexamethasone (DEX) are three examples of corticosteroids with established safety profiles, which have been used for the treatment of ocular inflammatory diseases. Since corticosteroids are hydrophobic drugs with extremely poor solubility in water, it is desired to solubilize them before loading into GelPatch. To address this issue, the encapsulation of hydrophobic drugs in nanocarriers has widely been described [19-21]. The desired drug carrier should be small, surface hydrophilic, and net-neutral surface charge in order to be incorporated into GelPatch. In addition, the drug carrier should also have a hydrophobic core to load hydrophobic drugs and enable sustained release. Polymeric micelles (MCs) consisting of a hydrophilic shell and a hydrophobic core are excellent candidates to deliver hydrophobic drugs [22, 23]. Several polymeric MC-based ocular drug delivery systems with sustained release have been reported recently [24, 25]. Biodegradable poly(ethylene glycol)-b-poly[N-(2-hydroxypropyl) methacrylamide-lactate] mPEG-b-p(HPMAm-Lac_n) diblock copolymers have been successfully used to deliver hydrophobic drugs for cancer therapy [27, 28, 36], but their use for the encapsulation of corticosteroids for ocular drug delivery has not been studied yet.

The aim of this study is to develop anti-inflammatory drug eluting patches which facilitate drug penetrating through the structural barriers of ocular tissues by adhering to the ocular surface and

providing a sustained release of drugs directly to the injured sites. To this end, we came up with the idea of solubilizing drugs in mPEG-b-p(HPMAm-Lac_n) polymeric MCs, which feature in drug protection and sustained release. These MCs were loaded inside hydrogel adhesive GelPatch with optimized adhesion, swelling ratio, and mechanical properties to be suitable on ocular tissues while retaining high *in vitro* and *in vivo* cytocompatibility. *In vitro* release profiles with and without the presence of enzymes were also assessed. Lastly, *in vivo* tests were conducted using a rat subcutaneous implantation model to study the biocompatibility and biodegradation of MC loaded GelPatch adhesives.

CHAPTER II. Materials and Methods

2.1. Materials

4,4-azobis(4-cyanopentanoic acid) (ABCPA), poly(ethylene glycol) methyl ether (Mw 5000 g/mol) (mPEG), N,N'-Dicyclohexylcarbodiimide (DCC), 4-dimethylaminopyridine (DMAP), and p-toluenesulfonic acid, L-lactide, N-(2-hydroxypropyl)methacrylamide (HPMAm), Tin(II) 2-ethylhexanoate ($SnOct_2$), and 4-methoxyphenol were purchased from Sigma-Aldrich. All solvents: tetrahydrofuran (THF), dichloromethane (DCM), dimethylformamide (DMF), acetonitrile (ACN), and acetone were provided by Sigma-Aldrich or Fisher Chemical. Nuclear magnetic resonance (NMR) solvents: chloroform-d ($CDCl_3$), deuterated dimethyl sulfoxide (DMSO-d6) and deuterium oxide (D_2O) were purchased from Cambridge Isotope Laboratories, Inc. Gelatin from porcine skin (Gel strength 300, type A), methacrylic anhydride, hyaluronic acid sodium salt from Streptococcus equi, glycidyl methacrylate (GM), Eosin Y disodium salt, triethanolamine (TEA) and N-vinylcaprolactam (VC), Triton X-100 were all purchased from Sigma-Aldrich.

2.2 Synthesis of micelles

2.2.1 Synthesis of macroinitiator $mPEG_2$-ABCPA

Macroinitiators $mPEG_2$-ABCPA were synthesized through an esterification of mPEG and ABCPA using DCC as a coupling reagent and 4-(dimethylamino)pyridinium 4-toluenesulfonate (DPTS, which was made by 1:1 molar ratio of DMAP and p-toluenesulfonic acid in THF) as a catalyst, as described in Bagheri et al [56]. In brief, 1 equiv of ABCPA (0.280 g), 2 equiv of PEG (10 g), and 0.3 equiv of DPTS (36.7 mg of DMAP and 57.3 mg of p-toluensulfonic acid each separately dissolved in 1 mL of THF) were dissolved in 50 mL of dry DCM with stirring on ice bath. Vacuum and nitrogen alternating cycles were repeated three times. Next, 3 equiv of DCC (0.619 g) were dissolved in 50 mL of dry DCM and dropwise added to PEG solution under nitrogen atmosphere. After the addition of DCC, the ice bath was removed allowing the mixture to react at room temperature. After 16 h, the reaction mixture was filtered to remove 1,3-dicyclohexyl urea salts and was dried under vacuum to remove solvents. Then, the remaining product was re-dissolved in water, stirred for 2 h, and dialyzed against water for 72 h at 4 °C. The final white product was obtained by freeze-drying and was analyzed by gel permeation chromatography **(**GPC) in DMF and proton nuclear magnetic resonance (^{1}H NMR) spectroscopy in $CDCl_3$.

2.2.2 Synthesis of monomer HPMAm-Lac_n

A mixture of 1 equiv of L-lactide (1 g), 1 equiv of HPMAm (0.993 g), 0.01 equiv of $SnOct_2$ (28.1 mg, 1 mol% relative to HPMAm), and 0.001 equiv of 4-methoxyphenol (0.86 mg, 0.1 mol% relative to HPMAm) were added in a round bottom flask [38]. Vacuum and nitrogen alternating

cycles were repeated three times to remove air. Then, the mixture was heated to 130 °C with stirring for 1 h and allowed to cool to room temperature.

The purification was done through a silica column chromatography. The reaction mixture was first dissolved in small amount of ethyl acetate (EtOAc) and dry-loaded on a silica column. 90% EtOAc/Hexane solvent system was used to run the column entirely. Thin Layer Chromatography (TLC) was used to analyze the separation. The fractions containing HPMAm-Lac_n were collected, and after solvent evaporation, the identity of obtained fractions was established by ^{1}H-NMR in $CDCl_3$. ^{1}H NMR for monomer HPMAm-Lac_n ($CDCl_3$, 400 MHz): Chemical shift (δ, ppm) = 6.32-6.04 (b, 1H, H_3), 5.71 (s, 1H, H_1), 5.35 (s, 1H, $H_{1'}$), 5.2-5.0 (m, H_5, H_8), 4.36 (q, 1H, H_9), 3.62 (m, 1H, H_4), 3.37 (m, 1H, $H_{4'}$), 1.96 (s, 3H, H_2), 1.50 (d, 6H, H_7, H_{10}), 1.27 (d, 3H, H_6).

2.2.3 Synthesis of copolymer mPEG-b-p(HPMAm-Lac_n)

The mPEG-b-p(HPMAm-Lac_n) was synthesized by radical polymerization using $mPEG_2$-ABCPA as macroinitiator and HPMAm-Lac_n as monomer, as described previously [57]. Monomer to macroinitiator feed ratio was 150:1. A mixture of HPMAm-Lac_n and $mPEG_2$-ABCPA were dissolved in dry ACN. The concentration of macroinitiator plus monomer was 300 mg/mL in ACN. The resulting solution was degassed by freeze-pump-thaw method and then heated to 70 °C with stirring for 24 h. After 24 h, the reaction was cooled to room temperature and diluted in a small amount of ACN (~2 mL). The product in the solution was precipitated by dropwise addition to an excess of cold diethyl ether (~45 mL) in a 50 mL vial. After centrifugation at 3000 rpm for 15 min, white pellet was obtained. Diethyl ether wash followed by centrifugation was repeated three times. Followed by dissolution in water, product solution was dialyzed (MWCO 12-14 kDa) against water and finally recovered by freeze drying. The final product was analyzed by GPC and ^{1}H-

NMR. ^{1}H NMR for copolymer mPEG-b-p(HPMAm-Lac$_n$) ($CDCl_3$, 400 MHz): δ = 6.6 (b, H_1), 5.3-4.8 (b, H_3, H_4), 4.39 (b, H_5), 3.64 (b, PEG CH_2-CH_2), 3.3-2.7 (b, H_2), 2.4-0.4 (the rest of the protons).

2.2.4 Preparation of unloaded and drug loaded micelles

Drug loaded MCs were formed by self-assembly via a solvent evaporation method as described before with modifications [56, 58]. Briefly, 10 mg of copolymers mPEG-b-p(HPMAm-Lac$_n$) were dissolved in 1 mL of acetone. Various amounts of drugs (0.25, 0.5, 1 and 2 mg) were then added to the copolymer solution and vortexed until fully mixed. Next, polymer/drug cocktail solution was quickly added to 1 mL of ammonium acetate buffer (120 mM, pH 5) with stirring. The mixture was stirred at room temperature for 30 min and then heated to 45 °C. After 2 h, the mixture was slowly cooled down to room temperature and stirred overnight. The next day, the MC solution was centrifuged at 4,000 rpm at 22 °C for 10 min to remove unencapsulated drugs. LE, PA, and DEX were three drugs of interest. 30 mg/mL of drug stock solutions were prepared in DMSO. Unloaded MCs were prepared with the same procedure without the addition of drugs.

2.3 Fabrication of GelPatch

2.3.1 Synthesis of GelMA

GelMA was synthesized as described previously [29]. In brief, 10% (w/v) gelatin from porcine skin (Bloom 300, type A, Sigma) was dissolved in Dulbecco's phosphate buffered saline (DPBS) and 8% (v/v) methacrylic anhydride was added dropwise at 55 °C. The mixture was allowed to react for 3.5 h under continuous stirring. The reaction was stopped by two times dilution in DPBS

and was dialyzed against water at 50 °C for 5 days. Finally, the resulting solution was frozen at -80 °C for 24 h and freeze-dried for 5 days to yield GelMA.

2.3.2 Synthesis of HAGM

Hyaluronic acid (HA) was modified with GM to form HAGM using a previously described protocol with some modifications [30, 31]. In brief, 1% (w/v) of HA (1.6 MDa, Sigma) was dissolved in 200 mL deionized water for 12 h under continuous stirring. After it fully dissolved, 8 mL triethylamine, 8 mL GM, and 4 g of tetrabutyl ammonium bromide (TBAB) were added in order separately and thoroughly mixed for 1 h before the next addition. Following complete dissolution, the reaction was allowed to continue overnight (16 h, 22 °C) and was finally completed by incubation at 60 °C for 1 h. After cooling to room temperature, the solution was then precipitated in 20 times excess volume of acetone (4 L) as white solid fibers. The precipitate was then dissolved in water, dialyzed for 2 days and lyophilized.

2.3.3 Preparation of unloaded and loaded GelPatch

GelPatch prepolymer was prepared by mixing GelMA and HAGM with a photoinitiator (PI) solution. This light-sensitive PI solution was prepared by dissolving 0.5 mM Eosin Y disodium salt, 1.86% (w/v) TEA and 1.25% (w/v) VC in phosphate buffered saline (PBS). 1 N hydrochloric acid was used to adjust the pH of PI solution to 8. Then, 7% (w/v) GelMA and 3% (w/v) HAGM were thoroughly mixed in PI solution and incubated at 50 °C overnight. After complete dissolution, the final GelPatch prepolymer solutions were crosslinked for 4 min with visible light (450 to 550 nm) by using an LS1000 Focal Seal Xenon Light Source (100 mW/cm^2, Genzyme). GelPatch containing free LE (GelPatch+LE) and GelPatch containing LE loaded MCs (GelPatch+MCLE)

were prepared with an additional step of physically mixing LE powder or MC solutions with dissolved GelMA and HAGM in PI solution before crosslinking.

2.4. Characterization

2.4.1 ^{1}H NMR spectroscopy and formulas

^{1}H NMR analysis of macroinitiator, monomer and copolymer

The ^{1}H NMR spectra of macroinitiator, monomer and copolymer were obtained in $CDCl_3$ using a Brucker AV 400 MHz NMR Spectrometer (2 sec delay and 64 scans). The chemical shift of $CDCl_3$ at 7.26 ppm was used as reference line. The average molecular weight of HPMAm-Lac$_n$ ($Mw_{ave\_HPMAm-Lac_n}$), the number of HPMAm-Lac$_n$ repeating units (m) and the average molecular weight of mPEG-b-p(HPMAm-Lac$_n$) (Mn) were determined by ^{1}H NMR, using the following equations:

(1) $$Mw_{ave\_HPMAm-Lac_n} = \%Lac_2 \times 287.31 + \%Lac_3 \times 359.38 + \%Lac_4 \times 431.44$$ (**Eq. 1**)

(2) $$m = \frac{I_{CO-CH(CH_3)-OH}}{I_{PEG_{5k}}/454}$$ (**Eq. 2**)

(3) $$Mn = Mw_{PEG_{5k}} + m \times Mw_{ave\_HPMAm-Lac_n}$$ (**Eq. 3**)

Where $I_{CO-CH(CH_3)-OH}$ is the value of the integration of the methine proton next to the hydroxyl group (Fig. 1D, H_5, δ = 4.39 ppm). $I_{PEG_{5k}}/454$ is the ratio of the integration of PEG$_{5k}$ proton to the average number of protons per PEG$_{5k}$ chain.

^{1}H NMR analysis of GelMA and HAGM

The gelatin and GelMA were dissolved in DMSO-d6 and HAGM was dissolved in D_2O at a concentration of 10 mg/mL and at a temperature of 50 °C. The ^{1}H NMR spectra were recorded with a Brucker AV 400 MHz NMR Spectrometer (10 sec delay and 64 scans). The degree of methacrylation (DM) of GelMA was defined as the ratio of methacrylate groups to the free amine groups in gelatin prior to the reaction [32, 33]. The vinyl protons on methacrylamide grafts gave rise to two peaks at δ = 5.62 and 5.29 ppm. The peak areas of methylene protons of lysine groups (δ = 2.75 ppm) in the spectra of gelatin and GelMA were integrated separately. The DM of GelMA was calculated from the following equation.

$$\mathrm{DM}\ (\%) = 1 - \frac{\mathrm{I_{lysine}(GelMA)}}{\mathrm{I_{lysine}(Gelatin)}} \times 100\% \ (\mathbf{Eq.4})$$

The DM of HAGM was defined as the amount of methacryloyl groups per one HA disaccharide repeating unit [30]. The two vinyl protons on methacrylate groups had chemical shifts of 6.16 and 5.16 ppm. The DM was calculated from the ratio of the relative peak integrations of the methyl protons of methacrylate groups (δ = 1.93 ppm) to the methyl protons of amide groups (δ = 2 ppm) on HA.

$$\mathrm{DM}\ (\%) = \frac{\mathrm{I_{H_3}\ (methyl\ Hs\ on\ GM)\ /\ 3}}{\mathrm{I_{H_4}\ (methyl\ Hs\ on\ HA)\ /\ 3}} \times 100\% \ (\mathbf{Eq.5})$$

2.4.2 Gel permeation chromatography (GPC)

Analysis of the $mPEG_2$-ABCPA macroinitiator and mPEG-b-p(HPMAm-Lac_n) copolymer was performed using a Waters System (Waters Associates Inc., Milford, MA) with refractive index (RI) using two serial PLgel 5 μm MIXED-D columns (Polymer Laboratories) and THF as eluent. The flow rate was 0.7 mL/min (45 min run time) and the temperature was 25 °C. The molecular weights of the synthesized polymers were determined by GPC analysis using RI detector and standards to calculate the number average molecular weight (Mn), the weight average molecular weight (Mw), and polydispersity index (PDI; (Mw/Mn)).

2.4.3 Dynamic light scattering (DLS)

Freshly prepared micellar dispersions were diluted 25 times with 10 mM HEPES, pH 7.0 (final concentration 400 μg/mL) and their sizes were analyzed with a Malvern Zetasizer Nano dynamic light scattering. Standard operating procedure parameters: 10 runs, 10 sec/run, three measurements, no delay between measurements, 25 °C with 120 sec equilibration time. Collection parameters: S26 lower limit = 0.6, upper limit = 1000, resolution = high, number of size classes = 70, lower size limit = 0.4, upper size limit = 1000, lower threshold = 0.05, upper threshold = 0.01. Data is representative of three replicate measurements.

2.4.4 Zeta potential

Zeta potential of the MCs was determined using a Malvern Zetasizer Nano-Z (Malvern Instruments, Malvern, UK) with universal ZEN 1002 'dip' cells and DTS (Nano) software (version 4.20) at 25 °C. Zeta potential measurements were performed in 10 mM HEPES at pH 7.4 at a final polymer concentration of 400 μg/mL.

2.4.5 Transmission electron microscopy (TEM).

The sample preparation for cryo-TEM was performed in a temperature and humidity-controlled chamber using a fully automated vitrification robot (FEICo., Hillsboro, OR). A thin aqueous film of MC solution was formed on a Quantifoil R 2/2 grid (Quantifoil Micro Tools GmbH, Jena, Germany) at 22 °C and at 100% relative humidity. This thin film was rapidly vitrified by shooting the grid into liquid ethane. The grids with the vitrified thin films were transferred into the microscope chamber using a Gatan 626 cryo-transfer/cryo-holder system (Gatan, Inc., Pleasanton, CA). Micrographs were taken using a CM-12 transmission microscope (Philips, Eindhoven, The Netherlands) operating at 120 kV, with the specimen at -170 °C and using low-dose imaging conditions.

2.4.6 Determination of encapsulation efficiency and loading capacity

The amount of loaded drugs (LE, PA and DEX) in the polymeric MCs was determined by using High Performance Liquid Chromatography (HPLC). Taking LE as an example, after centrifugation of the MC solution, the unencapsulated LE pellet was redissolved in 1mL of ACN. The concentration of this solution was measured by HPLC using a 70-90% ACN/water gradient solvent system at 242 nm (60-80% gradient at 243 nm for PA and 50-80% gradient at 239 nm for DEX). LE dissolved in ACN (concentration from 0.1mg/ml to 1mg/ml) was used for calibration. The encapsulation efficiency (EE) and loading capacity (LC) were calculated as follows:

$$\mathrm{EE\%} = 1 - \frac{\text{amount of unloaded drugs}}{\text{amount of drugs used for loading}} \times 100\% \ (\mathbf{Eq.6})$$

$$\mathrm{LC\%} = 1 - \frac{\text{amount of unloaded drugs}}{\text{amount of copolymer used for loading}} \times 100\% \ (\mathbf{Eq.\ 7})$$

2.4.7 Mechanical characterization

For the unconfined compression test, 75 µL of hydrogel precursor solution was pipetted into a polydimethylsiloxane (PDMS) cylindrical mold (diameter: 6 mm; height: 2.5 mm). The resulting solution was photocrosslinked via exposure to visible light for 4 min. After photocrosslinking, the dimensions of the hydrogels were measured using a digital caliper. The compression tests were conducted using an Instron 5542 mechanical tester. The crosslinked hydrogel cylinders were placed between the compression plates and compressed at a rate of 1 mm/min until failure. The slope of the stress-strain curves was obtained and reported as the compression modulus (N = 3).

2.4.8 *In vitro* burst pressure test

Burst pressure resistance (i.e. Adhesion strength) of the composite hydrogel formulations was measured by using the ASTM F2392-04 standard according to a previously reported method [34]. Briefly, collagen sheet made out of porcine intestine (4 × 4 cm) was placed in between two stainless steel annuli from a custom-built burst pressure device, which consists of a metallic base holder, pressure meter, syringe pressure setup, and data collector. A hole (2 mm diameter) was created through the sheet and was sealed (photocrosslinked) by applying 30 µL of hydrogel precursor solution. Next, the airflow was applied into the system, and the maximum burst pressure was recorded until detachment from the collagen sheet or hydrogel rupture. The burst pressure resistant was measured using a pressure sensor connected to a computer. Three replicates were performed for each hydrogel sample.

2.4.9 Measurement of swelling ratio

Hydrogel samples were prepared as described in section 2.3.3. The weight of each hydrogel sample (N = 3) was measured following photocrosslinking and after 24 h in DPBS at 37 °C. The swelling ratio was then calculated according to the equation below, where W_0 is the weight of the sample just after photocrosslinking and W_1 is the final weight of the sample after 24 h incubation.

$$\text{Swelling ratio } (\%) = \frac{W_1 - W_0}{W_1} \times 100 \ (\mathbf{Eq.8})$$

2.4.10 In vitro release profile from micelles and from GelPatch

The release profiles of LE, PA and DEX from the polymeric MCs were examined by a dialysis method [28]. Taking LE as an example, 1mL of LE loaded MC solution was pipetted into a dialysis bag (MWCO 12-14 kDa). The releasing medium was prepared with a solution of 2% Triton X-100 in DPBS. The dialysis bag was immersed in 10 mL of the releasing medium with stirring at 300 rpm at 37 °C. Samples (5 mL) of the receiving medium were drawn periodically and 5 mL of fresh releasing medium were added back to keep the volume constant. The concentration of LE in the different samples was measured using HPLC method mentioned in section 2.4.6. Calibration was done using LE (concentration from 0.005 mg/mL to 0.1 mg/mL) in 2% Triton X-100 in DPBS.

In vitro release profiles of LE from GelPatch+MCLE and GelPatch+LE were measured using the same releasing medium. A 250 µL of GelPatch+MCLE precursor solution was pipetted into cylindrical mold and photocrosslinked for 4 min. The gel cylinder was then immersed in 10 mL of releasing medium (2% Triton X-100 in DPBS) in an incubator shaker at 75 rpm at 37 °C. Samples (5 mL) of the receiving medium were drawn periodically and fresh releasing medium were added back to keep the volume constant. The concentration of LE in the different samples (N = 3) was

measured by HPLC. Additionally, *in vitro* release profile in the presence of enzymes were studied by adding 5 µg/mL of collagenase and 5 µg/mL of hyaluronidase on top of 2% Triton X-100 releasing medium with all other procedures remaining the same.

2.4.11 *In vitro* biocompatibility of GelPatch and MC loaded GelPatch (GelPatch+MC)

hTCEpi cells were cultured at 37 °C and 5% CO_2 in KBM™ basal media (00192151) supplemented with KGM-Gold™ Keratinocyte SingleQuots™ Kit (00192152). The cells were seeded on the surface of the hydrogel scaffolds as defined elsewhere [35]. Briefly, 10 µL of GelPatch precursor solutions were spread and photocrosslinked on a 3-(trimethoxysilyl) propyl methacrylate (TMSPMA)-coated glass slide, providing 1 x 1 cm^2 surface areas of hydrogels. Samples ($N \geq 3$) were placed in 24 well-plate and hTCEpi cells were seeded on the hydrogel surface (10^5 cells per sample). After incubation of the seeded samples in a humid incubator with 5% CO_2 for 20 min at 37 °C, 400 µL of media was added to each well and incubated. The media was replaced with fresh media every other day.

The viability of cultured cells on the gel scaffolds at day 1 and day 3 was evaluated using a Live/Dead™ Viability/Cytotoxicity Kit (Invitrogen) as stated by the manufacturer's instructions. Briefly, a solution of calcein AM at 0.5 µL/mL (green color, viable cells) and ethidium homodimer at 2 µL/mL (red color, non-viable cells) in DPBS was used to stain the cells. After 15 min of incubation, samples were washed with DPBS, and cells were imaged using a fluorescence optical microscope (Primovert, Zeiss). The collected images were analyzed using ImageJ software to quantify the cell viability (%) by dividing the number of live cells by the total number of live and dead cells.

Proliferation and metabolic activity of cells were determined using a PrestoBlue assay (Invitrogen) at day 1, 3, and 7 after culture according to the manufacturer's instructions. Briefly, seeded samples were incubated with a media solution containing 10% PrestoBlue reagent for 45 min with 5% CO_2 at 37 °C. The Fluorescence intensity of the solution was determined using a plate reader (BioTek) at 540 nm (excitation)/600 nm (emission).

The morphology of the cells and their expansion were assessed through staining of F-actin filaments with Alexa Fluor 594−phalloidin (Invitrogen) to visualize the cytoskeleton and cell nuclei with DAPI. Briefly, cells were fixed by incubating with 4% (w/v) paraformaldehyde for 15 min, then permeabilized using 0.3% (v/v) Triton in DPBS for 10 min and blocked with 1% (w/v) bovine serum albumin (BSA) in DPBS for 30 min at room temperature. Samples were serially incubated with phalloidin (1:400 dilution in 0.1% BSA) and DAPI (1:1000 dilution) solution for 45 min and 1 min, respectively. The samples were washed and imaged using the Zeiss fluorescent microscope.

2.4.12 *In vivo* studies on GelPatch and GelPatch+MC

Subcutaneous implantation in rats

All the *in vivo* studies were approved by the ICAUC (protocol 2018-076-01C) at University of California Los Angeles (UCLA). Male Wistar rats (200–250 gr) were purchased from Charles River Laboratories (Boston, MA, USA). Anesthesia was achieved by inhalation of isoflurane (2-2.5%), followed by subcutaneous meloxicam administration (5 mg/kg). After anesthesia, eight one-cm incisions were made on the dorsal skin of rats, and small subcutaneous pockets were made using a blunt scissor. GelPatch+MC, as well as pristine GelPatch as a control were formed using a cylindrical compression mold and then were lyophilized. The lyophilized hydrogels were

sterilized under UV light for 10 min. The sterile hydrogels were then implanted into the subcutaneous pockets, and incisions were closed with 4-0 polypropylene sutures (AD Surgical). At day 7 and 28 post-implantation, the rats were euthanized, and the hydrogels were explanted with the surrounding tissues for histological assessment.

Histological analyses were performed on the explanted hydrogels to investigate the inflammatory responses caused by the implanted hydrogels. After explantation of the samples with the surrounding tissues, they were fixed in 4% (v/v) paraformaldehyde for 4 h and incubated in 15% and 30% sucrose, respectively (at 4 °C, overnight). Samples were then embedded in Optimal Cutting Temperature compound (OCT), frozen in liquid nitrogen, and sectioned by using Leica CM1950 cryostat machine. Sections (8 µm thickness) were mounted on positively charged glass slides using DPX mountant (Sigma) for Hematoxylin and Eosin (H&E) staining and Masson's Trichrome (MT) staining, and ProLong™ Gold antifade reagent (Thermo fisher scientific) for immunofluorescence (IF) staining. The slides were then processed for H&E and MT staining (Sigma) according to manufacturer instructions. IF staining was also performed on mounted samples as previously reported. Anti-CD68 (ab125212) (Abcam) was used as primary antibody, and Goat-anti Rabbit IgG (H+L) secondary antibody conjugated to Alexa Fluor® 594 (Invitrogen) was used as a detection reagent. All samples were then stained using 4′,6-diamidino-2-phenylindole (DAPI) and the imaging was performed using ZEISS Axio Observer Z1 inverted microscope.

2.4.13. Statistical analysis

Results were presented as means ± SD (*P < 0.05, **P < 0.01, ***P < 0.001 and ****P < 0.0001). One-way or two-way analysis of variance (ANOVA) t test was performed followed by Tukey's test for statistical analysis (GraphPad Prism 8.0).

CHAPTER III. Results and Discussion

3.1. Synthesis and characterization of copolymer

Diblock copolymer mPEG-b-p(HPMAm-Lac_n) composed of a hydrophobic HPMAm-Lac_n block and a hydrophilic mPEG block was synthesized by radical polymerization with macroinitiator $mPEG_2$-ABCPA in a high yield of 80% (Fig. 1A). The monomer HPMAm-Lac_n was synthesized by ring-opening oligomerization of L-lactide using $SnOct_2$ as a catalyst. The monomer mixtures were purified through silica column chromatography to remove residual HPMAm and obtain a mixture of HPMAm-Lac_2 to HPMAm-Lac_4 as a light-yellow oil. From ^{1}H NMR spectrum, the percentage of HPMAm-Lac_2, HPMAm-Lac_3 and HPMAm-Lac_4 were calculated to be 41%, 38% and 21%, respectively, based on the integration ratio of amide protons (-NH-) in 6.1~6.3 ppm region (Fig. 1B). In addition, the PDI (Mw/Mn) of copolymer was measured to be 1.46 from GPC (Fig. 1C), which was within standard values for polymers that were synthesized by free radical polymerization [27]. The length of the hydrophobic block in copolymer was determined by the repeating units of HPMAm-Lac_n. The average repeating units were calculated to be 32 using equations mentioned in section 2.4.1 (Eq. 2) and therefore, by adding the weight of mPEG block, the average molecular weight of the copolymer was estimated to be 17,139 Da from ^{1}H NMR

spectrum (Fig. 1D). The synthesized mPEG-b-p(HPMAm-Lac$_n$) copolymers were then used as building blocks to form MCs, which solubilize our selected anti-inflammatory drugs.

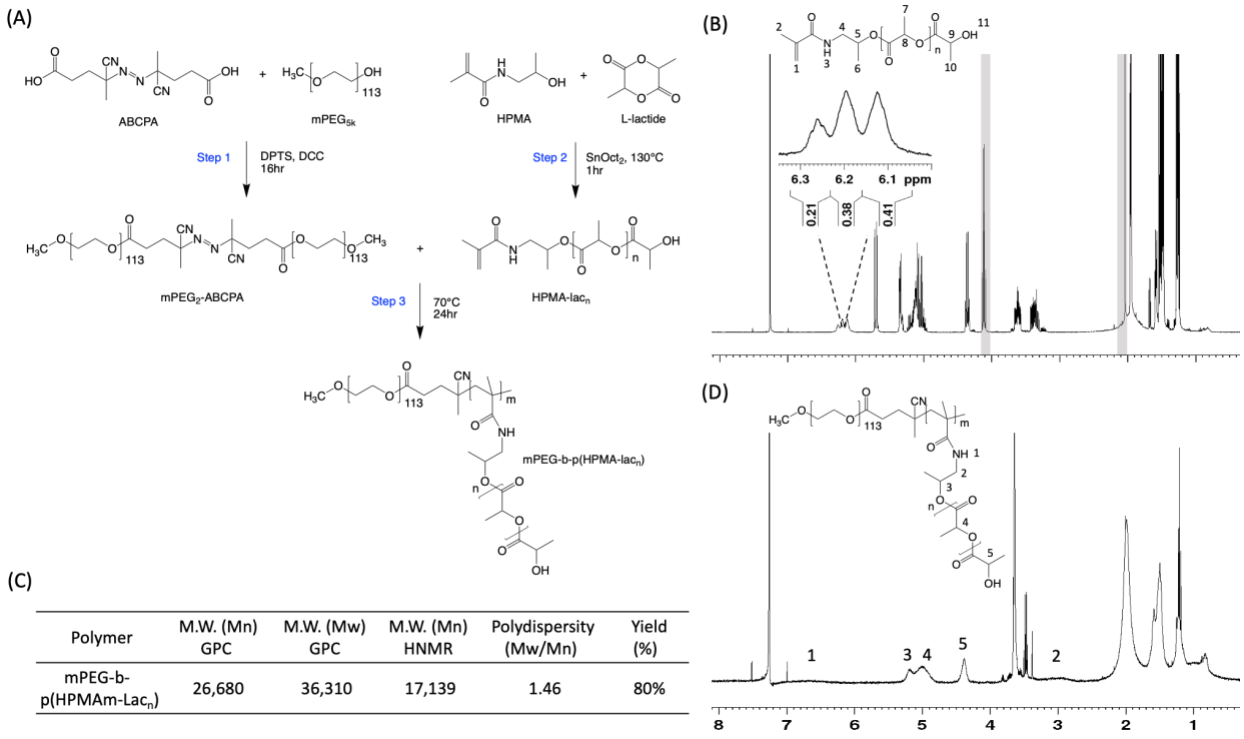

(C)

Polymer	M.W. (Mn) GPC	M.W. (Mw) GPC	M.W. (Mn) HNMR	Polydispersity (Mw/Mn)	Yield (%)
mPEG-b-p(HPMAm-Lac$_n$)	26,680	36,310	17,139	1.46	80%

Figure 1. Synthesis and characterization of mPEG-b-p(HPMAm-Lac$_n$) copolymer. A) A three-step synthetic scheme of mPEG-b-p(HPMAm-Lac$_n$) copolymer. B) ^{1}H NMR spectrum of HPMAm-Lac$_n$ monomer. C) Yield, GPC and ^{1}H NMR characterization of copolymer: the number average molecular weight (Mn), the weight average molecular weight (Mw), polydispersity (Mw/Mn). D) ^{1}H NMR spectrum of mPEG-b-p(HPMAm-Lac$_n$) copolymer.

3.2. MC formation and core interaction with corticosteroids

In previous studies, mPEG-b-p(HPMAm-Lac$_n$) MCs were successfully synthesized and used to solubilize several hydrophobic therapeutics, such as paclitaxel, vitamin K and an MRI contrast agent [26, 36, 37]. mPEG-b-p(HPMAm-Lac$_n$) MCs were shown to have tunable biodegradability

due to the hydrolysis of the lactate side chains under physiological conditions, which enabled sustained release of loaded therapeutics via diffusion [38]. In addition, PEG shell of MCs offered several advantages including drug protection, prolonged circulation, and reduced macrophage uptake, and their small size allowed better tissue penetration and facilitated overcoming physiological barriers [24, 59]. There were many studies shown their application in cancer therapy [27, 28, 36]. Herein, for the first time, we utilized mPEG-b-p(HPMAm-Lac_n) MCs to solubilize hydrophobic anti-inflammatory drugs for the treatment of ocular injuries.

MCs were formed by self-assembly via a solvent evaporation method [39]. mPEG-b-p(HPMAm-Lac_n) copolymers were firstly dissolved in acetone and were added to aqueous ammonium acetate buffer solution. During the evaporation of acetone, amphiphilic copolymers formed core-shell structures with hydrophobic HPMAm-Lac_n block clustering away from aqueous phase and hydrophilic mPEG orienting towards aqueous phase [40]. The average size of unloaded MCs was 109.0 ± 9.16 nm with a PDI of 0.094 ± 0.01 measured by DLS (Fig. 2A). In addition, the surface charge of unloaded MCs was -5.2 ± 0.96 mV measured by Zetasizer. The MCs were in a spherical shape and had similar size distribution shown in the TEM image (Fig. 2B). On a macroscopic view, the MC solution was transparent and showed slightly blue color because of light scattering by small MC particles (Fig. 2C) [41].

The table in Fig. 2D summarized the physical properties and structures of three corticosteroids which were loaded inside the engineered MCs. These are FDA-approved anti-inflammatory drugs to treat ocular anterior segment diseases [42-44]. LE, PA and DEX have similar core structures with different functional groups attached to the cyclopentane ring in addition to a fluoride at the carbon 9 (C-9) position for DEX and a hydrogen at C-9 position for LE and PA [45]. All of three are lipophilic molecules (LogP > 0) and have extremely poor solubility in water (< 0.1 mg/mL).

Among these three drugs, LE has only one H-bond donor and the highest LogP (LogP = 3.08), which explains its lowest solubility in water (0.0005 mg/mL).

Drug loaded MCs were formed by an additional step of mixing drugs with the synthesized copolymers in acetone before encounter with the aqueous phase. During the process of acetone evaporation, free floating hydrophobic drugs were slowly clustered together with the hydrophobic blocks of copolymers to form drug loaded MCs. Drug loading was achieved via both H-bonding and hydrophobic interactions between the drugs and copolymers (Fig. 2E) [46]. The 2-h heating process accelerated molecule movement, which increased the likelihood of drugs interacting with hydrophobic blocks and getting loaded into the hydrophobic core of MCs.

(A)

Micelle characterization

Size (nm)	PDI	Charge (mV)
109.0±9.16	0.094±0.01	-5.2±0.96

(B)

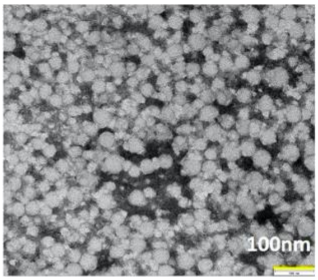

(C)

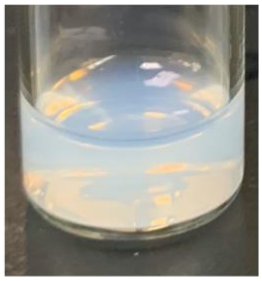

(D)

	Loteprednol Etabonate	Prednisolone Acetate	Dexamethasone
	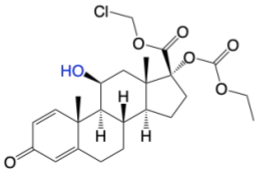	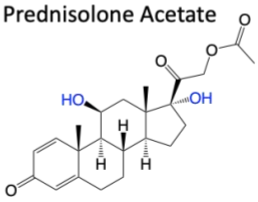	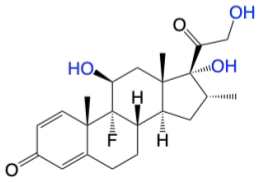
Solubility in water	0.0050 mg/mL	0.0417 mg/mL	0.0890 mg/mL
Lipophilicity LogP	3.08	2.17	1.93
H-bond donor	1	2	3
H-bond acceptor	5	5	5

(E)

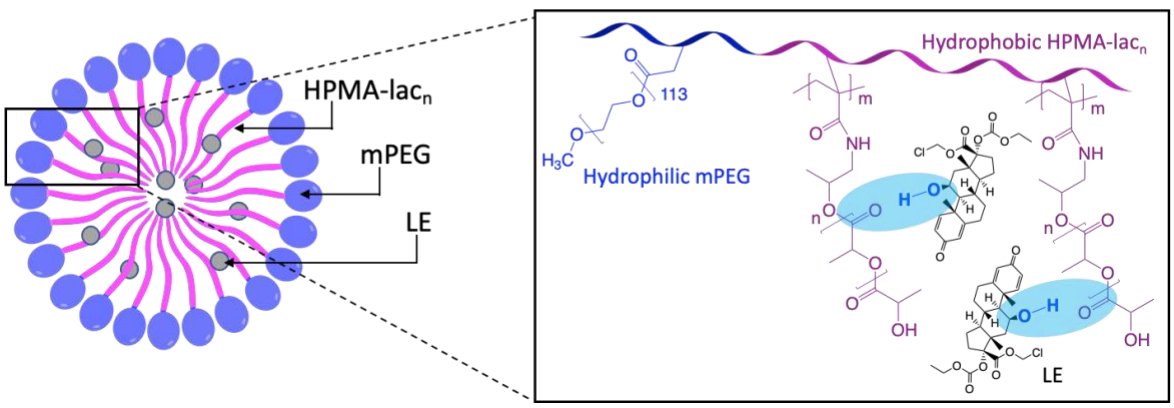

Figure 2. Micelle characterization, drug information and the schematic formation of drug loaded micelle. (A) The size (nm), PDI and surface charge (mV) characterization of unloaded mPEG-b-p(HPMAm-Lac$_n$) MCs. (B) A representative TEM image of unloaded MCs (scale bar, 100 nm). (C) Physical appearance of LE loaded MCs (copolymer/drug ratio (w/w) = 10:1). (D) The physical properties (solubility in water, lipophilicity LogP, H-bond donor and acceptor) and structures of three corticosteroids: LE, PA and DEX. (E) A schematic of LE loaded MCs with drug and copolymer interaction shown in the box.

3.3. Characterization of drug loaded MCs.

The quantity of drug loaded in the MCs varied with initial copolymer/drug ratios (w/w). For all drug candidates (LE, PA and DEX), various amounts of drug (0.25, 0.5, 1 and 2 mg) were mixed with a fixed 10 mg of copolymers to form drug loaded MCs. The final concentration of drug loaded in 1 mL of MC solution was measured by HPLC, and the results were shown in Fig. 3A. As the initial addition of drug increased from 0.25 mg to 2 mg, the final concentration of drug loaded inside MCs increased from 55.7 ± 10.0 μg/mL to 589.2 ± 75.5 μg/mL for LE, from 171.7 ± 4.2 μg/mL to 1154.0 ± 108.6 μg/mL for PA, and from 235.9 ± 5.0 μg/mL to 956.7 ± 150.3 μg/mL for DEX. On the other hand, there was no significant difference in EE% for LE and PA with various polymer/drug ratios while EE% for DEX decreased from 92.5 ± 1.7% to 47.8 ± 7.5% when the initial DEX added increased from 0.5 mg to 2 mg (Fig. 3B). Based on the results of loaded drug concentrations and EE%, we chose 10:1 polymer/drug ratio to move forward for size, PDI and surface charge characterization of drug loaded MCs. The sizes of drug loaded MCs were measured by DLS to be 117.30 ± 0.30 nm, 111.40 ± 0.94 nm and 84.30 ± 0.34 nm for LE, PA and DEX, respectively (Fig. 3C). We observed that due to the loading of LE and PA, the sizes of MCs containing drug became larger than the unloaded MCs (109.0 ± 9.16 nm) and the sizes of drug loaded MCs decreased as the number of H-bond donors on the drug increased. DEX loaded MCs had the smallest size among the three due to the most H-bonding interactions (H-bond donors = 3) between the hydroxyl groups on DEX and the ester oxygen of the hydrophobic MC core, which explained their smaller size than the unloaded MCs [28]. PDI values for all three drugs loaded MCs were small, 0.02 ± 0.01 (LE), 0.02 ± 0.01 (PA) and 0.03 ± 0.02 (DEX), which indicated

desired homogeneity and monodisperse of the MC system (Fig. 3D). The drug loaded MCs had net neutral surface charges (-0.24 ± 0.40 mV for LE, -0.59 ± 0.31 for PA, -0.27 ± 0.51 for DEX, Fig. 3E), which was desired for a slow degradation rate to serve as sustained drug release carriers [47]. In terms of EE% and LC% at 10:1 polymer/drug ratio, LE had an EE% of 25.5 ± 2.8% and a LC% of 2.5 ± 0.3% (Fig. 3F, 3G). PA and DEX had higher values of EE% 57.8 ± 2.1% and 74.6 ± 6.0% and higher values of LC% 5.5 ± 0.2% and 6.9 ± 0.5%, respectively. The results were aligned with our assumption that in addition to hydrophobic interactions, more H-bond donors on the drug supported more H-bonding interactions with hydrophobic core of MCs, which led to higher EE%, higher LC% and smaller MC size.

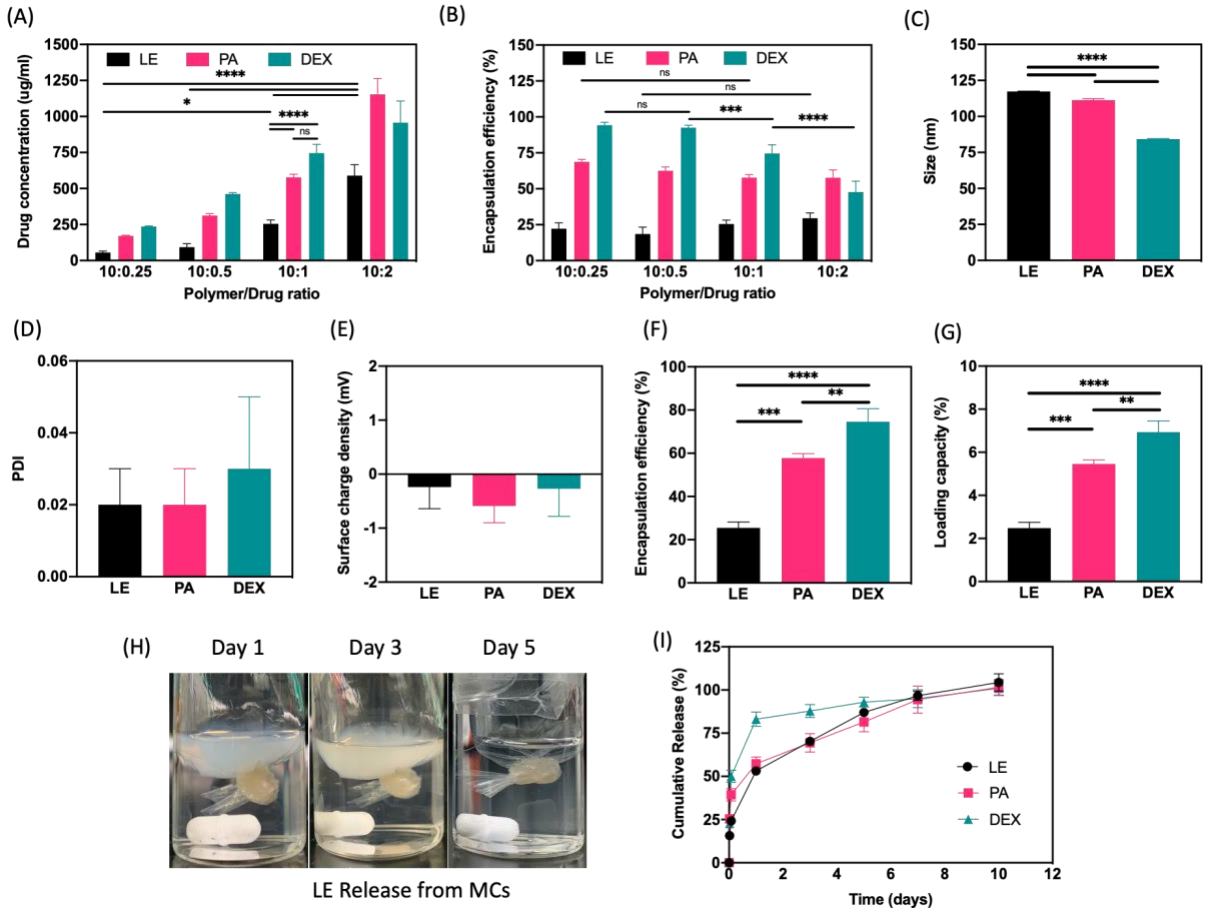

Figure 3. Drug loaded MC characterization. (A) The drug (LE, PA and DEX) concentrations in 1 mL of MC solution with different initial copolymer/drug ratios (w/w, 10:0.25, 10:0.5, 10:1 and 10:2). (B) EE%

for LE, PA and DEX with different initial copolymer/drug ratios (w/w, 10:0.25, 10:0.5, 10:1 and 10:2). (C) The size (nm) measurements, (D) PDI, (E) surface charge (mV), (F) EE%, and (G) LC% for LE, PA and DEX loaded MCs at the initial copolymer/drug ratio of 10:1. (H) The appearance of LE loaded MCs in the dialysis bag immersed in the releasing medium of 2% Triton X-100 in DPBS at 37 °C on day 1, 3 and 5. (I) Cumulative release of LE, PA and DEX from mPEG-b-p(HPMAm-Lac_n) MCs at 37 °C in the releasing medium of 2% Triton X-100 in DPBS measured by HPLC at different time points (30 min, 2 h, 1 day, 3 days, 5 days, 7 days and 10 days). Data are represented as means ± SD (*P < 0.1, **P < 0.01, ***P < 0.001, ****P < 0.0001, n = 3).

3.4. *In vitro* release of drugs from MCs.

One important aspect of this study was to achieve a sustained release of drugs to ocular surfaces in order to reduce the application frequency and improve patient compliance. To this end, *in vitro* release of LE, PA and DEX from MCs was assessed by a dialysis method [28]. Since LE, PA and DEX had extremely low aqueous solubility, it was difficult to maintain the molecular dispersion using DPBS buffer alone when drugs got released. A large amount of release media was required to keep drugs solubilized, but the drug concentration might be too low to be detectable by HPLC. Therefore, we added 2% Triton X-100 surfactant in DPBS buffer as the release media to better solubilize the released drugs [28]. Previous studies have confirmed that the addition of non-ionic surfactants did not induce MC destabilization and did not form mixed MCs due to the different chemical properties of surfactants and copolymers [48]. Fig. 3H presented the appearance change of LE loaded MCs submerged in the release media over 5 days. The visible light scattering properties of MCs altered over time as the size and integrity of MCs in the dialysis bag changed. This was likely due to the hydrolysis of the lactate chains of copolymers, which led to

hydrophilization and the swelling of the core of the MCs [38, 49]. It was found that LE, PA and DEX loaded mPEG-b-p(HPMAm-Lac$_n$) MCs released their full contents in around 10 days (Fig. 3I). An initial small burst release was observed for all three drugs with different extents. Specifically, DEX loaded MCs had the fastest initial release, where 50.0% of DEX was released after 2 h and 83.1% of DEX was released after 24 h. PA loaded MCs showed a slower release rate as compared to 39.4 % of PA release after 2 h and 57.3% after 24 h. LE loaded MCs showed the slowest release profile, where 24.2% of LE was released after 2 h and 53.1% after 24 h. The desired administration of topical corticosteroids is a small initial burst release and a gradual reduction over time [50]. LE loaded MCs satisfied the desired release profile among all the drugs without releasing too fast like DEX and PA. In addition, LE stands out from PA and DEX because it features an ester at the carbon 20 (C-20) position instead of a ketone [18]. The C-20 ester allows LE to be metabolized into inactive metabolites after exerting therapeutic effects, thereby avoiding adverse effects associated with intraocular pressure (IOP) relative to ketone-based corticosteroids [51, 52]. Therefore, we chose LE encapsulated MCs to be incorporated into the ocular adhesive hydrogel patch and further investigated its properties.

3.5. Fabrication and characterization of unloaded and MCs loaded GelPatch

Our ocular drug delivery platform, GelPatch, was a composite adhesive hydrogel made from methacrylated form of gelatin and hyaluronic acid which was loaded with the engineered MCs containing LE. ^{1}H NMR analysis was performed to determine the DM of GelMA and HAGM. Comparing ^{1}H NMR spectra of gelatin and GelMA, new peaks at δ = 5.62 and 5.29 ppm were corresponding to the two protons of methacrylate double bond (Appendix A1). In addition, the

decreased integration of lysine peaks at δ = 2.75 ppm further confirmed the reaction of gelatin with methacrylic anhydride [53]. The DM of GelMA was calculated to be 61% based on the percentage of consumption of lysine peaks (Eq. 4). On the other hand, HA was reacted with glycidyl methacrylate to form HAGM and the DM of HAGM was defined as the amount of methacrylate groups per one HA disaccharide repeating unit. The DM of HAGM was calculated to be 11% based on the ratio of the relative peak integration of methacrylate methyl protons (δ = 1.93 ppm) to HA's methyl protons (δ = 2.0 ppm) (Eq. 5, Appendix A2). The synthesized GelMA (7%, w/v) and HAGM (3%, w/v) were then mixed with the PI solution, which consisted of Eosin Y initiator, TEA and VC as described in previous work [54]. The mixture of GelPatch prepolymers was obtained as a viscous liquid. Finally, GelPatch hydrogel was formed by photocrosslinking the mixture under visible light for 4 min. To prepare GelPatch+MCLE, LE loaded MCs were physically mixed with dissolved GelMA and HAGM in PI solution before photocrosslinking as shown in Fig. 4A. Crosslinked hydrogel cylinders were obtained and used to evaluate the mechanical properties and *in vitro* swelling ratio.

The mechanical properties of GelPatch hydrogels were determined through compression tests (Fig. 4B, C, D). There was no significant difference in the maximum strain among GelPatch, GelPatch+LE and GelPatch+MCLE (Fig. 4C). However, the loading of free LE doubled the compression modulus from 10.30 ± 2.03 kPa to 22.39 ± 5.52 kPa, while the loading of LE loaded MCs did not significantly change the compression modulus which was measured as 13.02 ± 2.67 kPa. The increased compression modulus of GelPatch+LE indicated its increased stiffness. This was because undissolved LE remained as crystalline molecules inside GelPatch due to its poor aqueous solubility, whereas for GelPatch+MCLE, there was no solubility issue because MCs well

solubilized LE before loaded into GelPatch. Furthermore, the ultimate stress of GelPatch increased from 276.0 ± 15.52 kPa to 610.8 ± 215.43 kPa after the addition of LE loaded MCs and did not change after the addition of free LE. These results showed that the loading of MCs strengthened the resistance to the deformation of GelPatch hydrogels.

In addition to the characterization of mechanical properties, the swelling ratio was also evaluated. GelPatch itself had a swelling ratio of 15.38 ± 1.06% in DPBS at 37°C after 24 h. It was found that the addition of free LE and LE loaded MCs had no significant effect on the swelling ratio of GelPatch, and the values were measured to be 14.01 ± 2.81% and 17.32 ± 1.52% for GelPatch+LE and GelPatch+MCLE, respectively.

The adhesive strengths of the drug loaded/unloaded GelPatch were evaluated. The adhesive hydrogel can be used as the drug delivery matrix that can adhere to the ocular surface and directly deliver anti-inflammatory drugs to the site of inflammation. The current corticosteroids eye drops, however, are not adhesive and will be washed out by the tear film and blinking in a short period of time. Herein, *in vitro* burst pressure tests were performed based on a modified ASTM standard test (F2392-04) for GelPatch, GelPatch+LE and GelPatch+MCLE as described in section 2.4.8. The results showed that the burst pressure of GelPatch decreased from 27.7 ± 2.6 kPa to 19.35 ± 0.95 kPa after the addition of free LE and decreased to 11.6 ± 1.1 kPa after the addition of LE loaded MCs. The adhesion to collagen sheet, which was used as a biological substrate in this test, was due to the various chemical bond formation and physical interactions at the substrate/hydrogel interface. Although the addition of LE loaded MCs changed the intermolecular interactions within GelPatch as well as surface layer composition, which reduced the interface adhesion,

GelPatch+MCLE still maintained an improved adhesive strength compared to several commercially available surgical sealants such as Evicel, CoSEAL, Duraseal and fibrin sealant [54, 55].

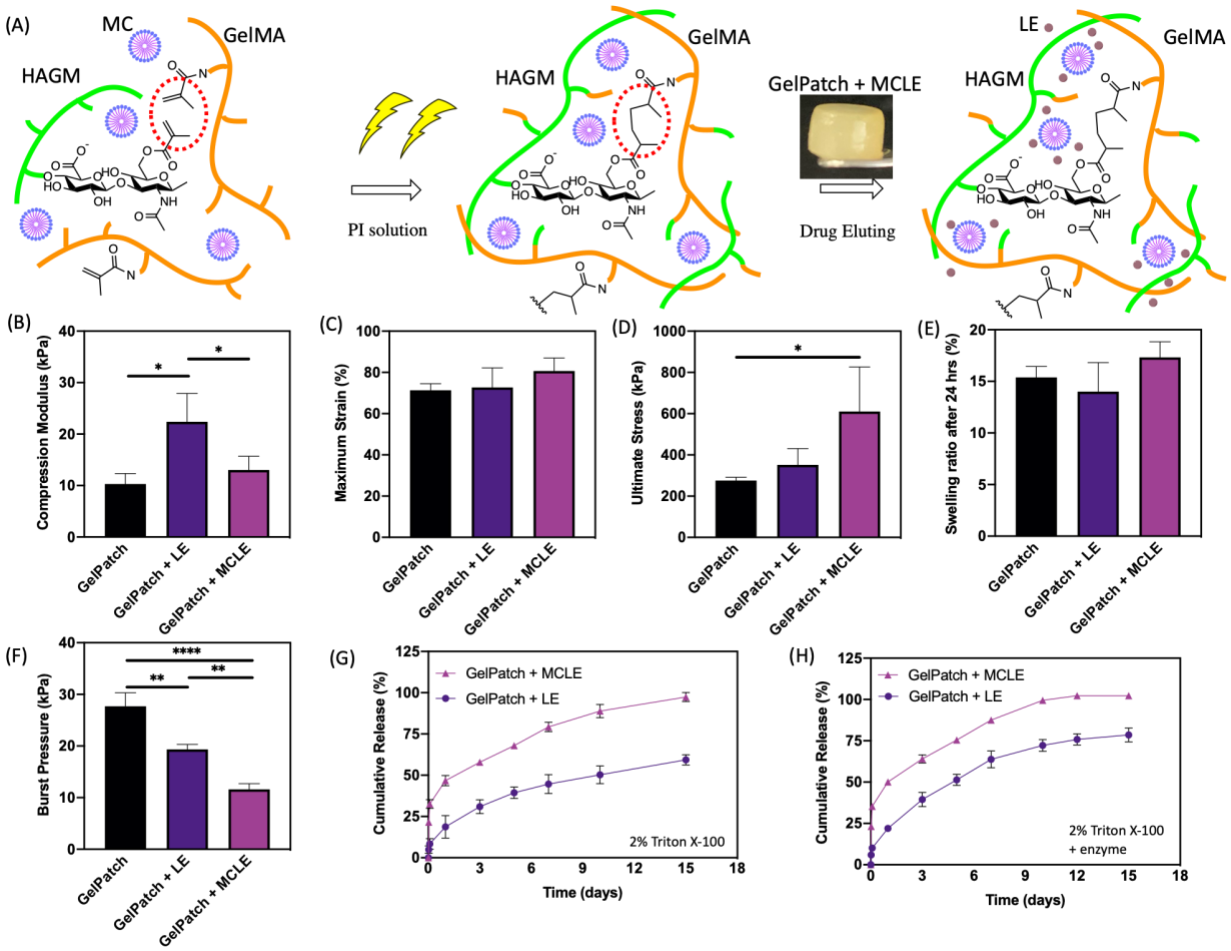

Figure 4. GelPatch formation and characterization. (A) Schematic of photocrosslinking of GelPatch+MCLE prepolymer solutions with the PI solution (Eosin Y, TEA and VC) and LE eluting from the crosslinked cylindrical hydrogel. (B) Compression modulus, (C) ultimate strain, (D) ultimate stress, (E) swelling ratio at 37 °C in DPBS after 24 h and (F) burst pressure of GelPatch, GelPatch+LE and GelPatch+MCLE fabricated using 7% GelMA and 3% HAGM (w/v) with 4-min photocrosslinking time. (G) *In vitro* release profiles of LE in 2% Triton X-100 releasing medium and (H) *in vitro* release profiles of LE in the presence of 5 μg/mL of collagenase and 5 μg/mL of hyaluronidase in 2% Triton X-100 releasing medium from GelPatch+LE and GelPatch+MCLE at 37 °C in 15 days. All hydrogels were

polymerized by using 0.5 mM Eosin Y, 1.875% (w/v) TEA and 1.25% (w/v) VC in PBS. Data are represented as means ± SD (*P < 0.1, **P < 0.01, ****P < 0.0001, n = 3).

3.6. *In vitro* release of LE from GelPatch

In vitro release profiles of LE from GelPatch+LE and GelPatch+MCLE were obtained in 2% Triton X-100 in DPBS with and without the presence of enzymes. Fig. 4G showed that 88.9% of LE was released from GelPatch+MCLE in 10 days and 100% was released after 15 days. On the other hand, only 50.2% of LE was released from GelPatch+LE in 10 days and 59.3% was released after 15 days. The slower release of LE from GelPatch+LE was due to the fact that LE remained in crystalline form inside GelPatch and its release was entirely based on the swelling and degradation of GelPatch by creating opportunities for Triton X-100 surfactant to solubilize LE into the releasing media. However, for the GelPatch+MCLE, the release of LE can be described as two continuous processes. LE loaded MCs were able to diffuse out slowly from GelPatch and then the hydrolysis of MCs happened in the release media where LE then got released. Simultaneously, the entrapped MCs could be hydrolyzed even slower within GelPatch and later LE would diffuse out from GelPatch directly. These two processes explained the slower LE release profile from GelPatch+MCLE compared to the LE release profile just from MCs. In order to assess the release profile in the presence of enzymes to mimic the real eye environment, we added 5 μg/mL of collagenase and 5 μg/mL of hyaluronidase in the 2% Triton X-100 release media. Fig. 4H showed that the overall release of LE in the presence of enzymes was faster from both GelPatch+LE and GelPatch+MCLE. 99.5% of LE was released from GelPatch+MCLE in 10 days and full release within 12 days; For GelPatch+LE, 72.2% of LE was released in 10 days and 78.5% after 15 days.

The increased release rate in the presence of enzyme was due to the faster enzymatic degradation of GelPatch, which resulted in decreasing polymer network density and increasing pore size. Therefore, MCs diffused out faster from GelPatch leading to a faster release of LE observed in Fig. 4H. The release profile data supported the study objective of the sustained release of anti-inflammatory LE to treat ocular injuries.

3.7. *In vitro* biocompatibility of the GelPatch scaffolds

To evaluate the biocompatibility of GelPatch and GelPatch+MC (without LE), the viability and metabolic activity of the seeded cells on the crosslinked gel samples were investigated through Live/Dead assay and PrestoBlue assay (at day 1, 3, and 7). The micrographs of stained cells by Live/Dead assay at day 1 and day 3 showed high viability of cells (>90%) seeded on both GelPatch+MC and GelPatch samples at the early stage of their culture (Fig. 5A, B). In addition, the morphology of the cultured cells on the hydrogels was evaluated using fluorescent staining F-actin in the cytoskeleton of cells on day 1 and day 3. The assembly of F-actin cytoskeleton of cells in fluorescent micrographs showed that the cells spread, adhered and proliferated on the surfaces of both GelPatch+MC and GelPatch samples, indicating the *in vitro* biocompatibility of the samples for cell adherence and growth (Fig. 5C). The metabolic activity of cultured hTCEpi cells on samples through PrestoBlue assay showed a consistent increase over 7 days without a significant difference to the control GelPatch group, which confirmed the biocompatibility of GelPatch+MC (Fig. 5D).

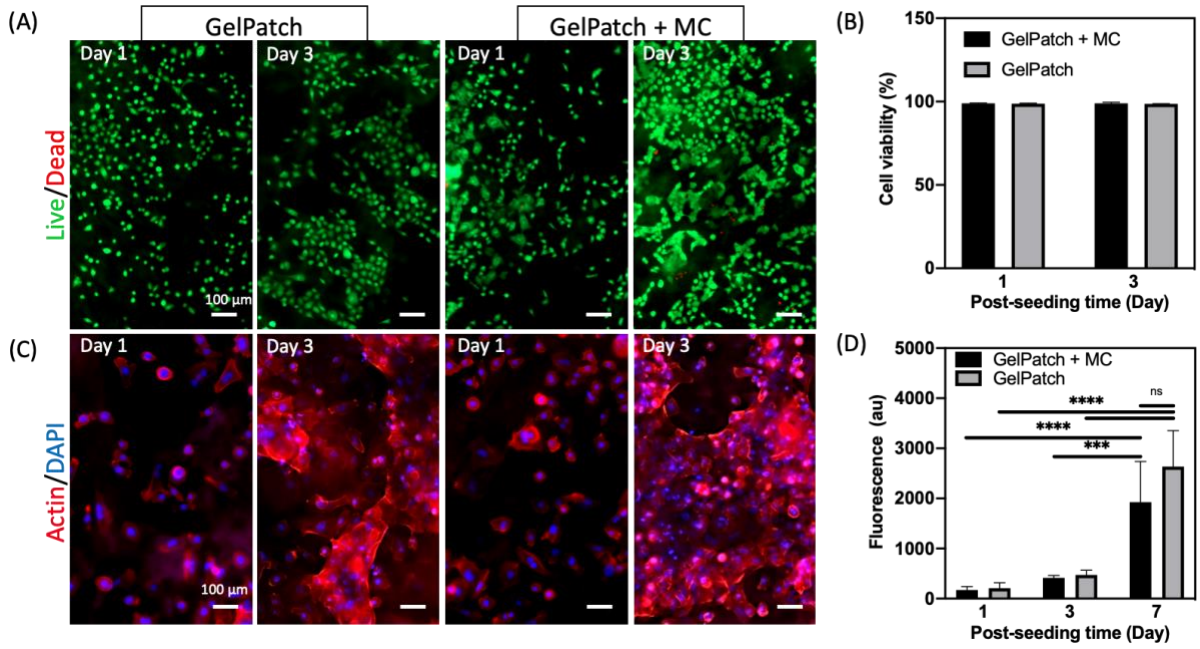

Figure 5. *In vitro* biocompatibility of GelPatch and GelPatch+MC. (A) Representative LIVE/DEAD images from hTCEpi cells seeded on hydrogels on day 1 and 3 (scale bar, 100 µm). (B) Quantification of cell viability on GelPatch and GelPatch+MC after 1 and 3 days of culture. (C) Representative Actin/DAPI images from hTCEpi cells seeded on hydrogels on day 1 and 3 (scale bar, 100 µm). (D) Quantification of metabolic activity of hTCEpi cells seeded on GelPatch and GelPatch+MC after 1 and 3 days. Data are represented as means ± SD (***P < 0.001, ****P < 0.0001, n ≥ 3).

3.8. *In vivo* biocompatibility and biodegradation of GelPatch and GelPatch+MC using a rat subcutaneous model

Lastly, subcutaneous implantations of GelPatch and GelPatch+MC in rats were performed to investigate their *in vivo* biocompatibility and biodegradation. The H&E staining images showed a small amount of cell infiltration in both GelPatch and GelPatch+MC (Fig. 6A). Based on MT staining in Fig. 6B, no significant fibrosis was detected in both hydrogels. In addition,

immunofluorescence analysis of subcutaneously implanted hydrogels demonstrated the presence of macrophages (CD68) at day 7, but they significantly reduced at day 28 (Fig. 6C). For *in vivo* biodegradation, our results suggested that there was no statistically significant change after 28 days, as demonstrated by visual inspection (Fig. 6D) and measurements in the weight loss of the samples (Fig. 6E). The large error bar seen in the percentage of weight loss of GelPatch samples (Fig. 6E) might be due to the variance of entrapment of adjacent tissues in the hydrogel samples, as the presence of red color shown in the images of the lyophilized hydrogels post-implantation (Fig. 6D). These results suggested that GelPatch encapsulated with MCs was biocompatible and was able to retain in a good shape after 28 days, which would allow sustained full release of drugs before GelPatch degraded.

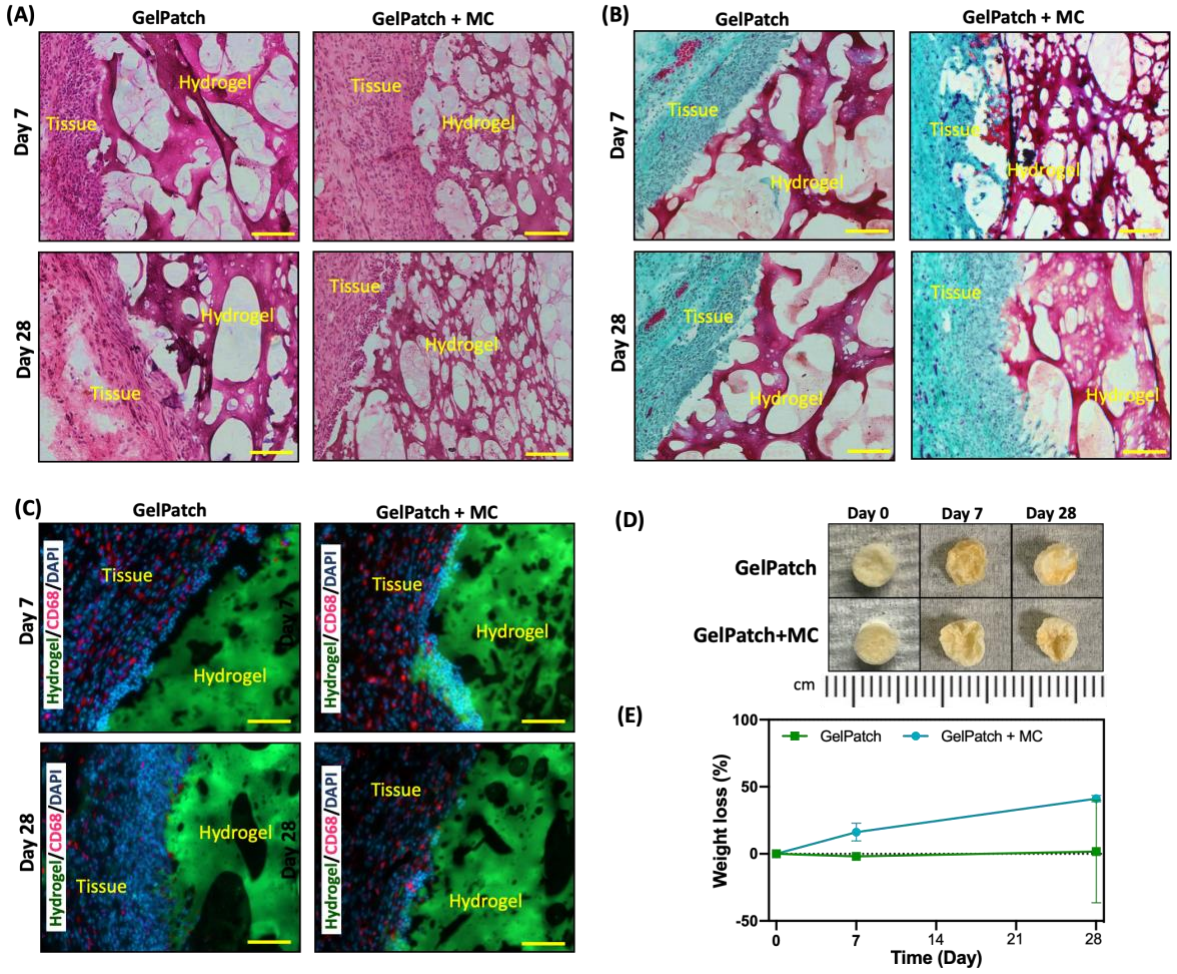

Figure 6. *In vivo* biocompatibility and biodegradability of GelPatch and GelPatch+MC using a rat subcutaneous model. (A) Hematoxylin and eosin (H&E) staining, (B) Masson's Trichrome (MT) staining, and (C) immunofluorescence (IF) staining images of GelPatch and GelPatch+MC sections (hydrogels with the surrounding tissue) after 7 and 28 days of implantation. (D) Representative images of GelPatch and GelPatch+MC hydrogels before implantation (day 0), on day 7 and 28 post-implantation. (E) *In vivo* biodegradation of hydrogels on day 7 and 28 post-implantation (scale bar, 100 μm). Data are represented as means ± SD.

CHAPTER IV. Conclusion

In this study, we developed anti-inflammatory drug eluting adhesive patches for treatment of ocular injuries. As drug carriers, mPEG-b-p(HPMAm-Lac_n) MCs successfully solubilized hydrophobic corticosteroids through H-bonding and hydrophobic interactions and provided sustained release of these drugs as demonstrated in the *in vitro* release studies. In addition, photocrosslinkable composite adhesive GelPatch showed appropriate mechanical strength, adhesion and swelling properties as ocular drug delivery platform. The incorporation of LE loaded MCs in GelPatch had no significant effect on the mechanical properties or the swelling properties of the composite hydrogel. Despite a small decrease in burst pressure, GelPatch+MCLE still maintained an improved adhesive strength compared to several commercially available surgical sealants and was able to achieve a sustained full release of LE in 15 days without enzymes and in 12 days in the presence of collagenase and hyaluronidase. Moreover, *in vitro* cell studies showed that MC loaded GelPatch had good biocompatibility and supported cellular adhesion, proliferation, and growth. *In vivo* studies further proved the *in vivo* biocompatibility and biodegradation of the engineered drug eluting adhesives to ensure the full release of anti-inflammatory drugs over 28

days. The developed non-invasive, adhesive and biocompatible GelPatch containing LE loaded MCs provides several advantages over conventional drug delivery methods such as improved patient compliance, site-targeted delivery, and lower dosage requirements, as well as circumventing the drawbacks of microneedles and current available adhesives. Despite the need for further *ex vivo* and *in vivo* adhesion studies on ocular tissues, the MC loaded GelPatch system had great capacity to incorporate other hydrophobic therapeutics and could become a promising ocular drug delivery platform for treatment of different ocular anterior segment diseases and injuries.

Appendices

A1. ^{1}H NMR spectrum of gelatin and GelMA

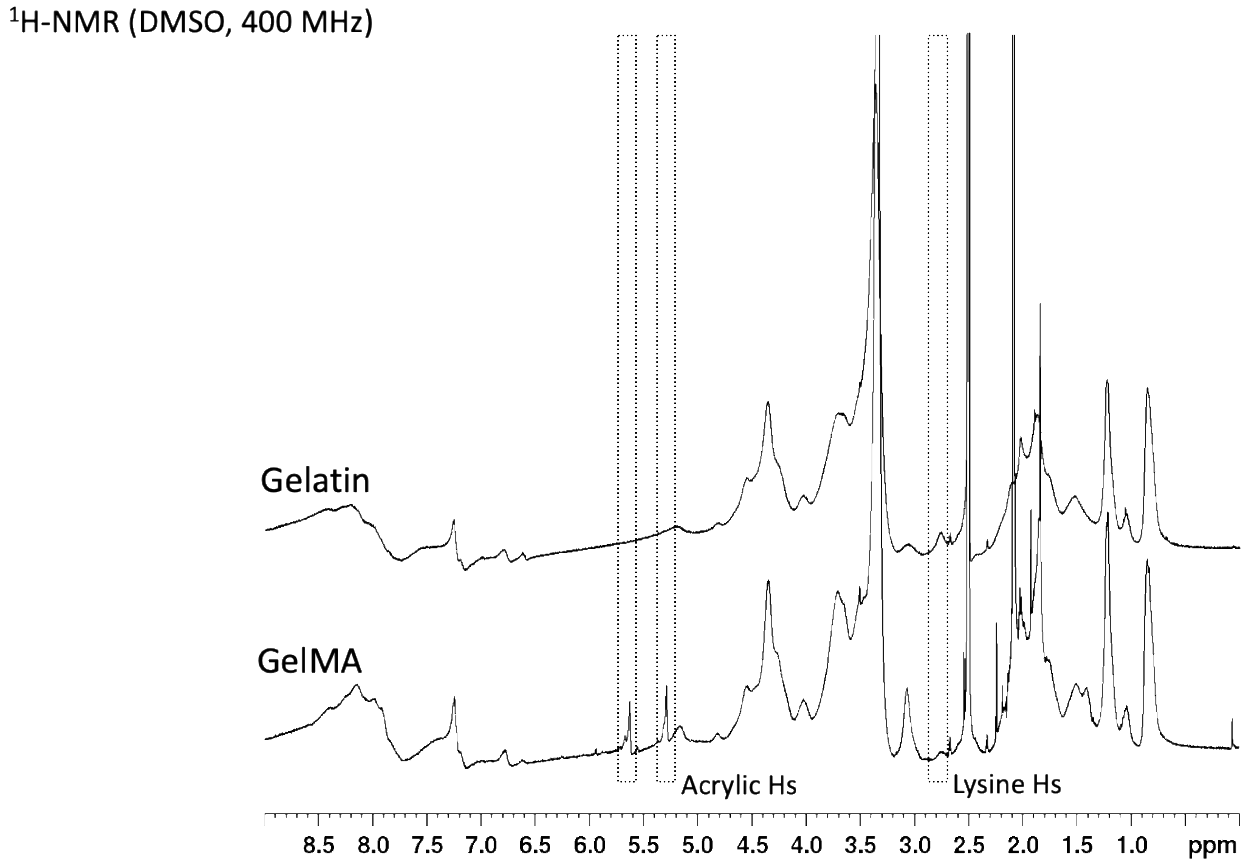

A2. ^{1}H NMR spectrum of HAGM

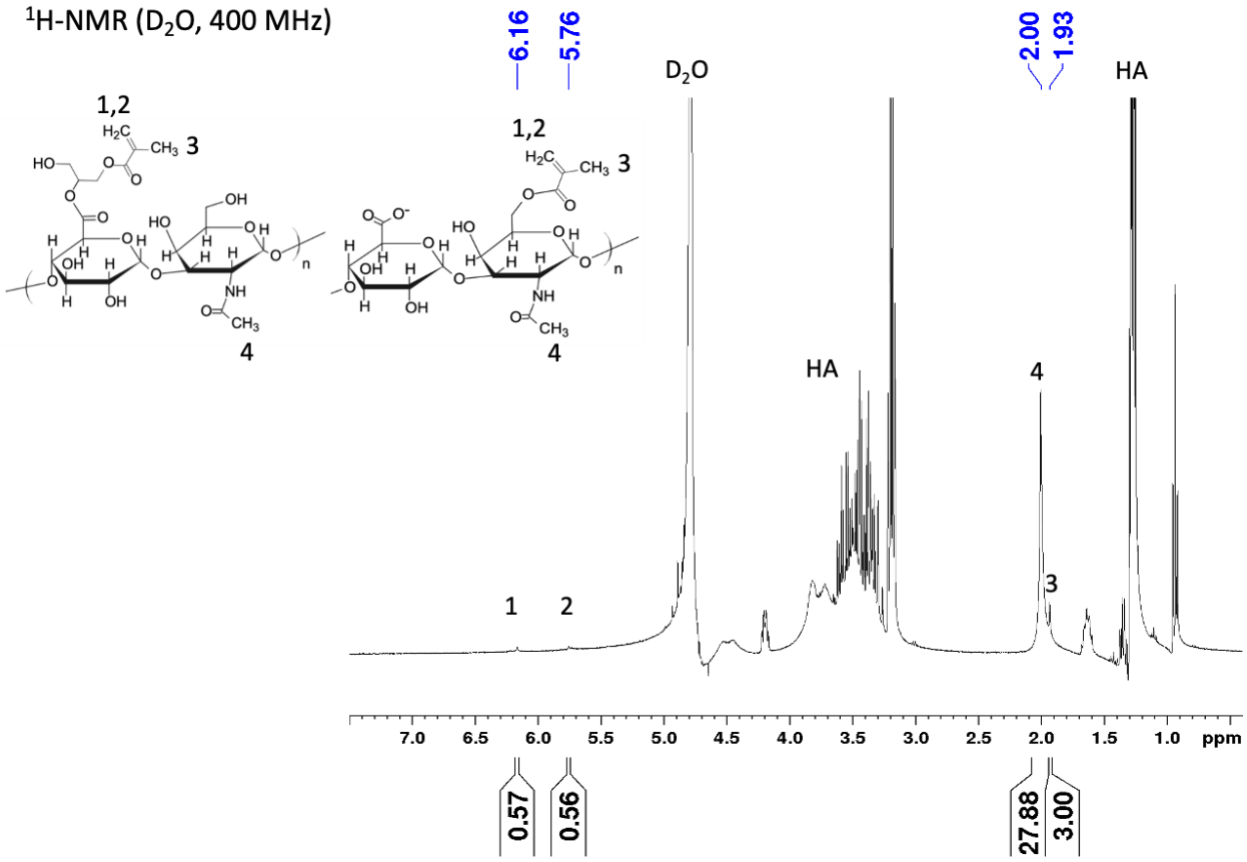

Bibliography

1. R. Klein, B. E. Klein, the prevalence of age-related eye diseases and visual impairment in aging: current estimates. *Invest Ophthalmol Vis Sci*. 54, ORSF5-ORSF13 (2013).
2. Y. C. Tham, X. Li, T. Y. Wong, H. A. Quigley, T. Aung, C. Y. Cheng, Global prevalence of glaucoma and projections of glaucoma burden through 2040: a systematic review and meta-analysis. *Ophthalmology.* 121, 2081-90 (2014).
3. M. L. Occhiutto, F. R. Freitas, R. C. Maranhao, V. P. Costa, Breakdown of the blood-ocular barrier as a strategy for the systemic use of nanosystems. *Pharmaceutics.* 4, 252-75 (2012).
4. A. Farkouh, P. Frigo, M. Czejka, Systemic side effects of eye drops: a pharmacokinetic perspective. *Clin. Ophthalmol.* 10, 2433-2441 (2016).
5. R. C. Cooper, H. Yang, Hydrogel-based ocular drug delivery systems: Emerging fabrication strategies, applications, and bench-to-bedside manufacturing considerations." *J. Controlled. Release.* 306, 29-39 (2019).
6. S. Kirchhof, A. M. Goepferich, F. P. Brandl, Hydrogels in ophthalmic applications. *Eur J Pharm Biopharm*. 95, 227-38 (2015).
7. R. R. Thakur Singh, I. Tekko, K. McAvoy, H. McMillan, D. Jones, R. F. Donnelly. Minimally invasive microneedles for ocular drug delivery. *Expert Opin. Drug Deliv*. 14, 525-537 (2017).
8. D. A. Goldstein, Achieving drug delivery via the suprachoroidal space. *Retina Today*. July/Aug (2014).
9. J. L. Alió, M. E. Mulet, J. C. Garcia, Use of cyanoacrylate tissue adhesive in small-incision cataract surgery. *Ophthalmic Surg. Laser*. 27, 270–274 (1996).
10. A. T. Trott, Cyanoacrylate tissue adhesives. An advance in wound care, *JAMA.* 277, 1559–1560 (1997).

11. G. Ciapetti, S. Stea, E. Cenni, A. Sudanese, D. Marraro, A. Toni, A. Pizzoferrato, Cytotoxicity testing of cyanoacrylates using direct contact assay on cell cultures. *Biomaterials* 15, 63–67 (1994).
12. S. S. Bhatia, Ocular surface sealants and adhesives. *Ocul Surf*. 4, 146–154 (2006).
13. B. Yanez-Soto, S. J. Liliensiek, C. J. Murphy, P. F. Nealey, Biochemically and topographically engineered poly(ethylene glycol) diacrylate hydrogels with biomimetic characteristics as substrates for human corneal epithelial cells. *J. Biomed. Mater. Res. A*. 101, 1184–1194 (2013).
14. ReSure Sealant. PMA P130004: FDA Summary of Safety and Effectiveness, (2014).
15. S. Masket, J. A. Hovanesian, J. Levenson, F. Tyson, W. Flynn, M. Endl, P. A. Majmudar, S. Modi, R. Chu, M. B. Raizman, S. S. Lane, T. Kim, Hydrogel sealant versus sutures to prevent fluid egress after cataract surgery. *J Cataract Refract Surg*. 40, 2057–2066 (2014).
16. G. Trujillo-de Santiago, R. Sharifi, K. Yue, E. Shrizael Sani, S. S. Kashaf, M. M. Alvarez, J. Leijten, A. Khademhosseini, R. Dana, N. Annabi. Ocular adhesives: Design, chemistry, crosslinking mechanisms, and applications. *Biomaterials* 197, 345-367 (2019).
17. G. Kogan, L. Soltés, R. Stern, P. Gemeiner, Hyaluronic acid: a natural biopolymer with a broad range of biomedical and industrial applications. *Biotechnol Lett*. 29, 17-25 (2007).
18. M. J. Coffey, H. H. Decory, S. S. Lane, Development of a non-settling gel formulation of 0.5% loteprednol etabonate for anti-inflammatory use as an ophthalmic drop. *Clin Ophthalmol*. 7, 299-312 (2013).
19. G. M. Nabar, K. D. Mahajan, M. A. Calhoun, A. D. Duong, M. S. Souva, J. Xu, C. Czeisler, V. K. Puduvalli, J. J. Otero, B. E. Wyslouzil, J. O. Winter, Micelle-templated, poly(lactic-*co*-glycolic acid) nanoparticles for hydrophobic drug delivery. *Int J Nanomedicine*. 13, 351-366 (2018).

20. Y. H. A. Hussein, M. Youssry, Polymeric Micelles of Biodegradable Diblock Copolymers: Enhanced Encapsulation of Hydrophobic Drugs. *Materials (Basel)*. 11, 688 (2018).
21. S. Gholizadeh, Z. Wang, X. Chen, R. Dana, N. Annabi, Advanced nanodelivery platforms for topical ophthalmic drug delivery. *Drug Discovery Tod*ay (2021).
22. P. S. Chan, J. W. Xian, Q. Li, C. W. Chan, S. S. Y. Leung, K. K. W. To, Biodegradable Thermosensitive PLGA-PEG-PLGA Polymer for Non-irritating and Sustained Ophthalmic Drug Delivery. *AAPS J.* 21, 59 (2019).
23. C. J. Rijcken, T. F. Veldhuis, A. Ramzi, J. D. Meeldijk, C. F. van Nostrum, W. E. Hennink, Novel Fast Degradable Thermosensitive Polymeric Micelles Based on PEG-block-poly (N-(2-hydroxyethyl) methacrylamide-oligolactates). *Biomacromolecules*. 6, 2343-51 (2005).
24. A. Mandal, R. Bisht, I. D. Rupenthal, A. K. Mitra, Polymeric micelles for ocular drug delivery: From structural frameworks to recent preclinical studies. *J Control Release*. 248, 96-116 (2017).
25. Y. Özsoy, S. Güngör, E. Kahraman, M. E. Durgun, "Polymeric micelles as a novel carrier for ocular drug delivery." *Nanoarchitectonics in Biomedicine*, pp. 85-117. William Andrew Publishing, 2019.
26. M. Talell, C. J. F. Rijcken, T. Lammers, P. R. Seevinck, G. Storm, C. F. van Nostrum, W. E. Hennink, Superparamagnetic iron oxide nanoparticles encapsulated in biodegradable thermosensitive polymeric micelles: toward a targeted nanomedicine suitable for image-guided drug delivery. *Langmuir*. 25, 2060-7 (2009).
27. M. Talelli, M. Iman, A. K. Varkouhi, C. J. F. Rijcken, R. M. Schiffelers, T. Etrych, K. Ulbrich, C. F. van Nostrum, T. Lammers, G. Storm, W. E. Hennink, Core-crosslinked polymeric

micelles with controlled release of covalently entrapped doxorubicin. *Biomaterials* 31, 7797-7804 (2010).

28. O. Naksuriya, Y. Shi, C. F. van Nostrum, S. Anuchapreeda, W. E. Hennink, S. Okonogi, HPMA-based polymeric micelles for curcumin solubilization and inhibition of cancer cell growth. *EUR J Pharm Biopharm.* 94, 501-512 (2015).
29. J. W. Nichol, S. T. Koshy, H. Bae, C. M. Hwang, S. Yamanlar, A. Khademhosseini, Cell-laden microengineered gelatin methacrylate hydrogels. *Biomaterials* 31, 5536-5544 (2010).
30. S. A. Bencherif, A. Srinivasan, F. Horkay, J. O. Hollinger, K. Matyjaszewski, N. R. Washburn, Influence of the degree of methacrylation on hyaluronic acid hydrogels properties. *Biomaterials* 29, 1739-49 (2008).
31. J. E. Prata, T. A. Barth, S. A. Bencherif, N. R. Washburn, Complex Fluids Based on Methacrylated Hyaluronic Acid. *Biomacromolecules 11*, 769-775 (2010).
32. H. Shirahama, B. H. Lee, L. P. Tan and N. J. Cho, Precise Tuning of Facile One-Pot Gelatin Methacryloyl (GelMA) Synthesis. *Sci Rep 6*, 31036 (2016).
33. L. Zhou, G. Tan, Y. Tan, H. Wang, J. Liao, C. Ning, Biomimetic mineralization of anionic gelatin hydrogels: effect of degree of methacrylation. *RSC Adv*. 4, 21997-22008 (2014).
34. E. Shirzaei Sani, R. Portillo-Lara, A. Spencer, W. Yu, B. M. Geilich, I. Noshadi, T. J. Webster, N. Annabi, Engineering adhesive and antimicrobial hyaluronic acid/elastin-like polypeptide hybrid hydrogels for tissue engineering applications. *ACS Biomater. Sci. Eng*. 4, 2528–2540 (2018).
35. I. Noshadi, S. Hong, K. E. Sullivan, E. S. Sani, R. Portillo-Lara, A. Tamayol, S. R. Shin, A. E. Gao, W. L. Stoppel, L. D. Black III, A. Khademhosseini, N. Annabi, In vitro and in vivo

analysis of visible light crosslinkable gelatin methacryloyl (GelMA) hydrogels. *Biomater Sci*. *5*, 2093-2105 (2017).

36. O. Soga, C. F. van Nostrum, M. Fens, C. J. F. Rijcken, R. M. Schiffelers, G. Storm, W. E. Hennink, Thermosensitive and biodegradable polymeric micelles for paclitaxel delivery. *J. Control. Release.* 103, 341–353 (2005).
37. P. M. van Hasselt, G. E. P. J. Janssens, T. K. Slot, M. van der Ham, T. C. Minderhoud, M. Talelli, L. M. Akkermans, C. J. F. Rijcken, C. F. van Nostrum, the influence of bile acids on the oral bioavailability of vitamin K encapsulated in polymeric micelles. *J. Control. Release.* 133, 161–168 (2009).
38. D. Neradovic, M. J. Van Steenbergen, L. Vansteelant, Y. J. Meijer, C. F. van Nostrum, W. E. Hennink, Degradation mechanism and kinetics of thermosensitive polyacrylamides containing lactic acid side chains. *Macromolecules* 36, 7491–7498 (2003).
39. Z. Jiao, X. Wang, Z. Chen, Advance of Amphiphilic Block Copolymeric Micelles as Drug Delivery. April 2013. *Asian J. Chem*. 25, 1765-1769 (2013).
40. R. Trivedi, U. B. Kompella, Nanomicellar formulations for sustained drug delivery: strategies and underlying principles. *Nanomedicine (Lond)*. 5, 485-505 (2010).
41. P. M. Carvalho, M. R. Felício, N. C. Santos, S. Gonçalves, M. M. Domingues, Application of Light Scattering Techniques to Nanoparticle Characterization and Development. *Front Chem*. 6, 237 (2018).
42. N. Patel, H. Nakrani, M. Raval, N. Sheth, Development of loteprednol etabonate-loaded cationic nanoemulsified *in-situ* ophthalmic gel for sustained delivery and enhanced ocular bioavailability. *Drug Deliv*. 23, 3712-3723 (2016).

43. Y. Ran, N. Jain, S. H. Yalkowsky, Prediction of Aqueous Solubility of Organic Compounds by the General Solubility Equation (GSE). *J. Chem. Inf. Comput. Sci. 41,* 1208-1217 (2001).

44. S. H. Yalkowsky, R. M. Dannenfelser, Aquasol database of aqueous solubility. *College of Pharmacy, Univ. of Ariz, Tucson, AZ* 189 (1992).

45. G. P. Moss, Nomenclature of steroids, recommendations 1989. *Pure Appl. Chem*. 61, 1783-1822 (1989).

46. X. Yang, B. Zhu, T. Dong, P. Pan, X. Shuai, Y. Inoue, Interactions between an anticancer drug and polymeric micelles based on biodegradable polyesters. *Macromol Biosci*. 8, 1116-25 (2008).

47. Y. Wan, Z. Gan, Z. Li, Effects of the surface charge on the stability of PEG-*b*-PCL micelles: simulation of the interactions between charged micelles and plasma components. *Polym. Chem*. 5, 1720-1727 (2014).

48. R. Khonkarn, S. Mankhetkorn, M. Talelli, W. Hennink, S. Okonogi, Cytostatic effect of xanthone-loaded mPEG-b-p (HPMAm-Lac2) micelles towards 740 doxorubicin sensitive and resistant cancer cells. *Colloids Surf. B. Biointerfaces* 94, 266–273 (2012).

49. O. Soga, C. F. van Nostrum, A. Ramzi, T. Visser, F. Soulimani, P. M. Frederik, P. H. H. Bomans, W. E. Hennink, Physicochemical characterization of degradable thermosensitive polymeric micelles. *Langmuir* 20, 9388–9395 (2004).

50. G. Rull, Anti-inflammatory eye preparations. Drug Therapy (2016).

51. N. Bodor, T. Loftsson, W. M. Wu, Metabolism, distribution, and transdermal permeation of a soft corticosteroid, loteprednol etabonate. *Pharm Res*. 9, 1275–1278 (1992).

52. N. Bodor, P. Buchwald, Soft drug design: general principles and recent applications. *Med Res Rev*. 20, 58–101 (2000).

53. I. A. Khalil, B. Saleh, D. M. Ibrahim, C. Jumelle, A. Yung, R. Dana, N. Annabi, Ciprofloxacin-loaded bioadhesive hydrogels for ocular applications. *Biomater. Sci*. 8, 5196-5209 (2020).

54. E. Shirzaei Sani, A. Kheirkhah, D. Rana, Z. Sun, W. Foulsham, A. Sheikhi, A. Khademhosseini, R. Dana, N. Annabi, Sutureless repair of corneal injuries using naturally derived bioadhesive hydrogels. *Sci Adv*. 5, eaav1281 (2019).

55. P. K. Campbell, S. L. Bennett, A. Driscoll, A. S. Sawhney, "Evaluation of absorbable surgical sealants: *in-vitro* testing." *In-vitro testing*, pp. 1170576081-1559295193 (2005).

56. M. Bagheri, J. Bresseleers, A. Varela-Moreira, O. Sandre, S. A. Meeuwissen, R. M. Schiffelers, J. M. Metselaar, C. F. van Nostrum, J. C. van Hest, W. E. Hennink, Effect of formulation and processing parameters on the size of mPEG-b-p (HPMA-Bz) polymeric micelles. *Langmuir*. 34, 15495-506 (2018).

57. M. Talelli, C. J. Rijcken, S. Oliveira, R. van der Meel, P. M. van Bergen En Henegouwen, T. Lammers, C. F. van Nostrum, G. Storm, W. E. Hennink, Nanobody-shell functionalized thermosensitive core-crosslinked polymeric micelles for active drug targeting. *J Control Release*. 151, 183-92 (2011).

58. H. M. Aliabadi, S. Elhasi, A. Mahmud, R. Gulamhusein, P. Mahdipoor, A. Lavasanifar, Encapsulation of hydrophobic drugs in polymeric micelles through co-solvent evaporation: the effect of solvent composition on micellar properties and drug loading. *International journal of pharmaceutics*. *329*, 158-165 (2007).

59. H. Cabral, K. Kataoka, Progress of drug-loaded polymeric micelles into clinical studies. *J Control Release*. 190, 465-476 (2014).